



<b>Project name:</b>	Structural Applications of Ferritic Stainless Steels
Project's short name:	SAFSS
Project number:	39594

**Work package 2:**  
**Model calibration tests – Members in fire**

**Barbara Rossi**  
University of Liège

## 1. Objectives

This Work Package seeks to obtain information on the performance of structural members made of ferritic stainless steel when exposed to fire loading. Column tests subjected to fire loading first and, second, at ambient temperature were carried out. Trusses and space frames made of tubular thin-walled members are typical structural typologies where ferritic stainless steel is employed. As a result, the experimental campaign focussed on such profiles that were tested under concentric compressive load. In detail, three fire tests on columns of varying global slenderness were carried out. In order to fully identify the effects of fire loading, identical columns were also tested at room temperature. In addition, mechanical properties at room temperature were established by means of tensile tests on material coupons extracted from members. Finally, numerical simulations were performed to reproduce the test results.

## 2. Tests at elevated temperature

### 2.1 Specimens geometry and boundary conditions

Three profiles made of ferritic 1.4003 were selected: i) two square hollow sections (SHS) 80 x 80 x 3 mm having nominal lengths of 3000 mm and 2500 mm, respectively; and ii) a rectangular hollow section (RHS) 120 x 80 x 3 mm, 2500 mm long. This choice entailed the SHS to be classified as class 2 according to the EN1993-1-4 (2006) and the RHS as class 4.

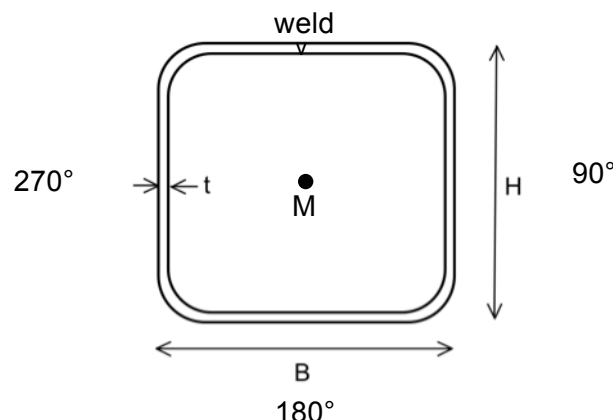


Figure 1. Notations for the cross-section dimensions

From a fire behaviour viewpoint, the three columns have a massivity factor that is fairly the same and rather high (Table 1). The massivity factor is the ratio between the area (or perimeter) exposed to fire and the volume (or the area) of the member. The higher the massivity factor the higher is the rate of temperature increase in the section.

Due to the fact that small variations in the geometry may highly influence the response of thin-walled members, the actual dimensions were accurately measured before each test and for the specimens tested under fire, they are reported in Table 1; where  $t_{av}$  is the average of the thicknesses of the four faces. The out-of-straightness of the four faces was also measured and this was the only indication of the initial imperfection. For columns #1 and #2, the maximum amplitude was less than 1 mm. Only column #3 had an initial maximum out-of-straightness equal to 5.0 mm (at mid-height), i.e. about  $L/500$ .

The cross-section areas were calculated on the basis of an average measured corner internal radius  $R_i$  of 4.0 mm for the 80 x 80 x 3 sections and 3.86 mm for the 120 x 80 x 3 section as follows

$$A = 2t_{av} \left[ B + H - 4(R_i + t_{av}) \right] + \pi(R_i + t_{av})^2 - \pi R_i^2$$

**Table 1 Specimen dimensions (notations on Figure 1)**

#	1	2	3
<b>Section [mm]</b>	80 x 80 x 3	80 x 80 x 3	120 x 80 x 3
<b>Length [mm]</b>	3000.0	2499.5	2500.0
<b>Maximum global imperfection amplitude [mm]</b>	< L/3000	< L/2500	~L/500
<b>Cross-section measured dimensions [mm]</b>	$t_{av} = 2.87$ $B = 79.6$ $H = 79.2$	$t_{av} = 2.82$ $B = 79.2$ $H = 79.8$	$t_{av} = 2.97$ $B = 79.4$ $H = 119.5$
<b>A [cm<sup>2</sup>]</b>	8.5	8,4	11.2
<b>Massivity factor [m<sup>-1</sup>]</b>	360	365	345

The specimens were welded to 20 mm thick end plates (see Figure 2) made of stainless steel grade 1.4307 and holes for bolts were allowed for to ensure a full degree of fixity at both column ends. In fact, all tests were conceived with double fix-end conditions. The welding wire was made of 1.4430 stainless steel grade. The depth of the welded lips was 5.0 mm thick.



**Figure 2. Left to right – bottom end plate with holes for bolts, supporting concrete block with waiting steel bars, column top end with plate mounted on the concrete block**

## 2.2 Tests on material at room temperature

The employed stainless steel grade was of ferritic type 1.4003. This grade exhibits similar mechanical properties to traditional carbon steel. The main room-temperature mechanical characteristics of this grade, according to EN 10088-2 (2005), are: (i) 0.2% proof strength  $\sigma_{0.2\%} \geq 280$  MPa, (ii) elongation after fracture  $\epsilon_{ult} \geq 20\%$  and (iii) ultimate tensile strength  $\sigma_{ult} = 450$  to 650 MPa. The specimens were supplied by the steelwork company Stalalube that provided the mill certificates for both sections, see Table 2 and Appendix 1.

Tensile coupon tests at room temperature on material coupons from the members were also carried out by Aperam (Interim Technical Report) in order to establish the mechanical properties. Three tests were performed in accordance with EN 10002 (2004). The coupons were extracted from each of the three faces: namely 90°, 180° and 270°, as illustrated in

Figure 1. The face that included welding was excluded. Coupons were cut out of the flat sides of the tubes and tested in an Instron 5582 electromechanical testing machine. Up to 1% elongation the test was carried out in load control with stress rate of 20 MPa/s. Then, it continued in displacement control at strain rate of 40% $L_0$ /min; where  $L_0$  is the initial specimen length. Young's modulus was computed in the loading phase between 0.03% and 0.07% elongation. The mill certificate data and average tensile coupon tests properties are provided in Table 2 and Table 3. The full stress-strain curves are given in Appendix 2.

**Table 2 Mill certificate data (from Stalatube)**

Section	80 x 80 x 3	120 x 80 x 3
$\sigma_{0.2}$ [MPa]	336.0	329.0
$\sigma_{1.0}$ [MPa]	360.5	350.0
$\sigma_{ult}$ [MPa]	484.5	468.0
$\epsilon_{ult}$ [%]	42.5	37.0

**Table 3 Average tensile coupon tests results (from Aperam)**

Section	80 x 80 x 3	120 x 80 x 3
$\sigma_{0.2}$ [MPa]	458.7	437.2
$\sigma_{1.0}$ [MPa]	485.8	462.8
$\sigma_{ult}$ [MPa]	505.4	490.1
$\epsilon_{ult}$ [%]	25.6	24.2
$E_0$ (MPa)	193	194

Cold-formed structural sections are manufactured at ambient temperature and hence undergo plastic deformations, which result in an increase in yield stress and a reduction in ductility. Square and rectangular hollow sections are first formed into a circular section than further crushed into a square or a rectangular cross-section. Materials, such as stainless steel, with rounded stress-strain behaviour and significant strain hardening show a more pronounced response to cold working. Compared to the mill certificate data, the tensile coupon tests indicate that the flats experienced hardening especially the face situated in front of the weld (180° in Figure 1) because of the bending sequences. It is explicable by the fact that in addition to the bending curvature enhanced by the whole cross-section during fabrication into a circular hollow section, the inferior face is also bent in the opposite direction (see the bending sequence development depicted in Figure 3). This may also significantly harden the base material and lead to a higher strength and lower ductility (Rossi et al., 2013).

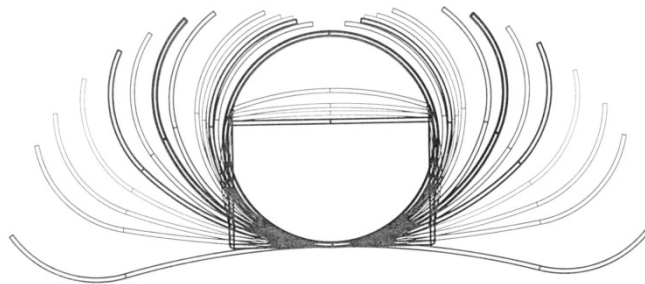


**Figure 3. Bending sequences occurring during the manufacture of a rectangular hollow section (credit: L. Faivre Aperam)**

## 2.3 Test set-up and loading protocol

The columns were tested in the vertical wall furnace at the Fire Testing Laboratory of the University of Liege, the competence of which is certified by the accreditation to the ISO 17025 standard delivered by the Belgian accreditation body BELAC. The furnace is provided with a system capable to impose vertical loads to the specimens. The bottom horizontal beam (HEB 400) can move up along slide guides attached to the columns of the reaction frame (Figure 4). These guides basically allow only the translational displacement (up and down). Slight rotation about the horizontal transverse axis of the beam may however occur owing to connection slacks. In fact, for the three tests, a small adjustment was observed at the beginning of the static loading then both displacement transducers (left and right) provided the same measure indicating that the lower support did not rotate. The load was transmitted to the column through the lower beam connected by means of two jacks, as depicted in Figure 4.

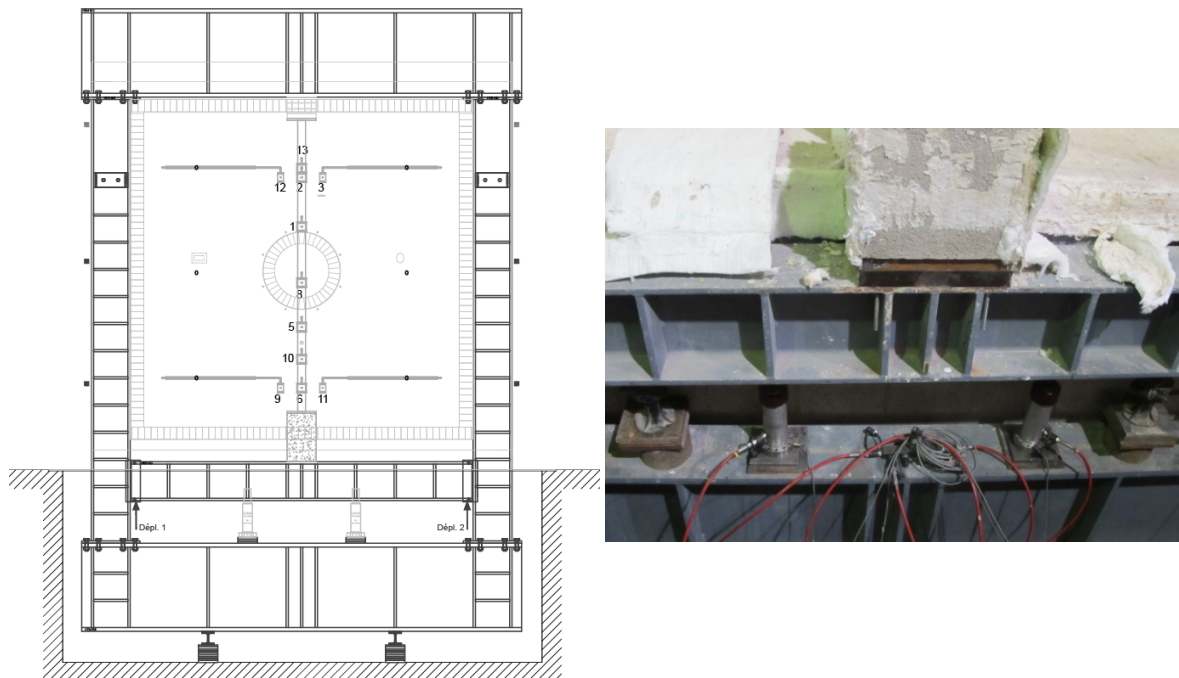


**Figure 4. Left to right – schematic elevation of the vertical furnace, lower beam with left and right jacks**

The plates bolted to the concrete blocks were covered with a fine grain temperature resistant plaster to guarantee an optimal contact with the plate (Figure 2). The interior volume of the furnace was then covered with ceramic fibre including the supports made of concrete. Therefore, the heated length reduced of approximately 50 mm (the fibre is 25 mm thick, Figure 5).

The distribution of the air temperature (as well as oxygen and pressure) in the furnace was measured by using pyrometers located at 11 points around the column: 7 coming into the furnace through the closing device and 4 located behind the column coming into the furnace through the brick wall where burners are located (Figure 5). They provided the air temperature at a distance of 100 mm from the steel surface. No thermocouples were installed on the specimens because it was reckoned that due to the small thicknesses, the temperature of steel at failure could be sensibly considered equal to that of air.



The load protocol followed the EN1363-1 provisions (2001) which entail to maintain the load constant at least during 15 minutes, time after which the ISO 834 heating curve is applied, with the load being maintained constant until failure. In detail, the tests began by applying the static loading at ambient temperature until 30% of the design load  $N_{b,Rd}$  calculated according to EN1993-1-4 (2006) (see Table 4). In this table, the design load is calculated on the basis of a yield strength equal to 350MPa.



**Figure 5. Left to right – column top end covered with ceramic fibre, 4 pyrometers located at the back side of the column, 7 pyrometers located at the front side of the column through the furnace closing device**

**Table 4 Applied load**

#	1	2	3
<b>Section [mm]</b>	80 x 80 x 3	80 x 80 x 3	120 x 80 x 3
<b>Length [mm]</b>	3000.0	2499.5	2500.0
<b>Heated length [mm]</b>	2950.0	2449.5	2450.0
$N_{b,Rd}$ [kN]	239	260	336
<b>Applied load [kN]</b>	72	78	100

Transversal displacements are usually not measured and, so, the mode of failure is generally only visible on the screen during the test or after opening the furnace at the end of it. When possible, one pyrometer is replaced with one displacement transducer but it is always very difficult to predict the direction of the movement (backward or inward buckling) or even to analyse it when torsional buckling occurs. Moreover, by having square sections the eventual direction of failure cannot be predicted a priori.

Presently, we measured the transverse displacements by replacing two (out of 11) pyrometers with two ceramic stalks (located at 1429 mm from the bottom end of column #1 and at 1319 mm from the bottom of columns #2 and #3) and oriented at forty degrees from the column faces, see Figure 7. The displacement transducers (located outside the furnace)

measured the movements of the stalks that were connected to the column by means of two bolts (*dépl. 3* and *dépl. 4*, see Figure 6 and Figure 7). Those two measures are relevant only at the beginning of the loading when they remain sufficiently low, i.e. when the measure along the stalk equals the transversal component.

After the static loading at ambient temperature was applied, the fire test began according to the ISO 834 fire curve. It is worth pointing out that *time zero* conventionally means the time at which the temperature inside the furnace reaches 50°C. The temperature curve is defined using 16 points. A small deviation from the required curve is always observed at the beginning of the test because the change of temperature of the ISO curve is too fast to be followed by burners, see Figure 8. In fact, no tolerances are provided in EN1363-1 for the first 5 min. The deviation occurred in the test was measured and it respected the given tolerances (see Appendix 3 for column #1).

The failure time was defined from  $t = 0$ , defined by the EN1363-1 provisions (2001), to the time when the displacements increased with vertical asymptote. This information is useful to determine the fire resistance of the members subjected to the prescribed axial load.

It is important to mention that, as described before, a closing wall was necessary in order to seal the wall furnace during the tests. This means that a gradient of temperature may develop horizontally inside the furnace, causing the columns to get warmer on the side toward the hot bricks composing the furnace wall, the one which contains the gas burners. This gradient may influence the direction of buckling and the overall behaviour (Tondini et al., 2013).

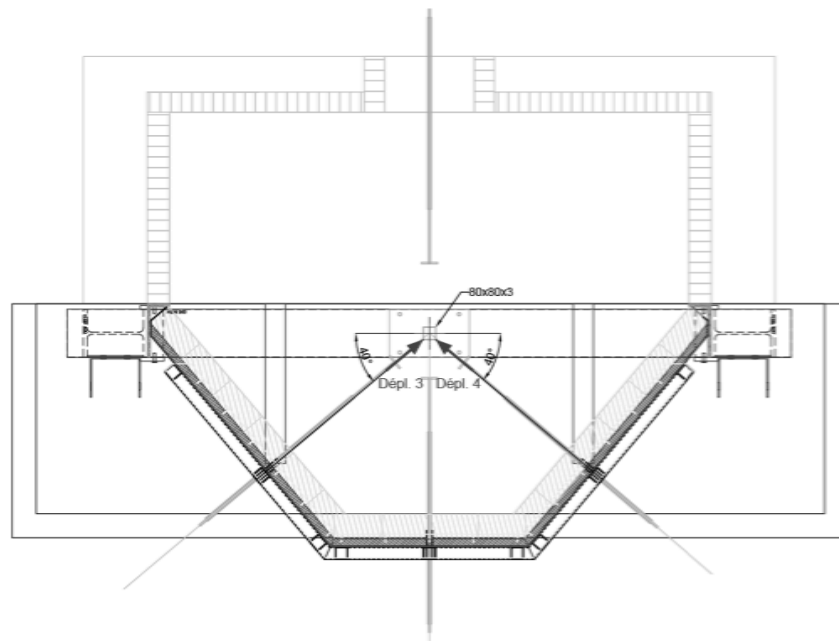


**Figure 6. Schematic plan of the vertical furnace (seen from above), indicating where and how the transverse displacements (*dépl. 3* and *dépl. 4*) are measured**



Figure 7. Left to right: displacement transducers placed to measure transverse displacement; a detail of bolts used to support them

## 2.4 Main test results

In this section the main results for the three tests subjected to fire loading are presented. For each test, the evolution of the air temperature compared to the ISO 834 standard curve; the axial displacement given as the average of left and right displacements; the failure time and the failure mode are reported. Load versus time curves are given in the Appendix 4.

### 2.4.1 Column #1

From Figure 9 it is possible to observe that the axial displacement was first positive owing to elastic shortening of the column at ambient temperature. Then, when the fire test began it became negative because of thermal expansion.

The time of failure occurred at 12 min 9 s after *time zero* and at the air temperature of 709.4 °C.

Figure 10 shows column #1 after being tested. The failure mode involved the formation of a main plastic hinge at the column centre and, less developed, at about a quarter and at two quarters of the height. Thus, full *fixed-end* boundary conditions seemed to be achieved.



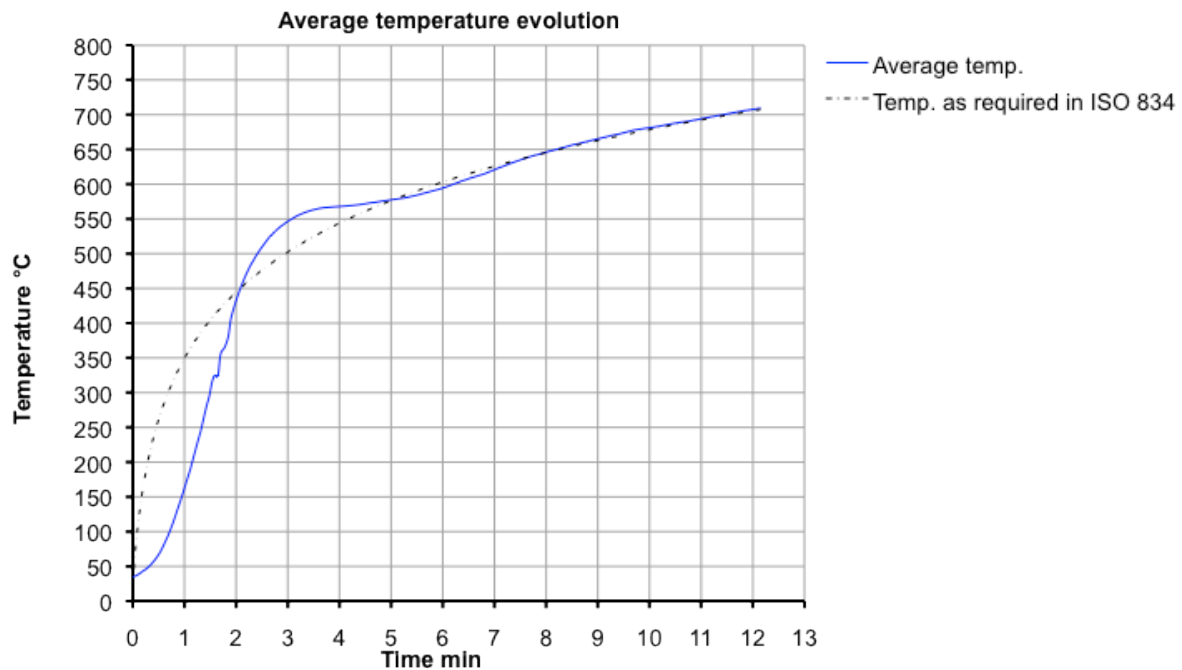


Figure 8. Average air temperature evolution for column #1

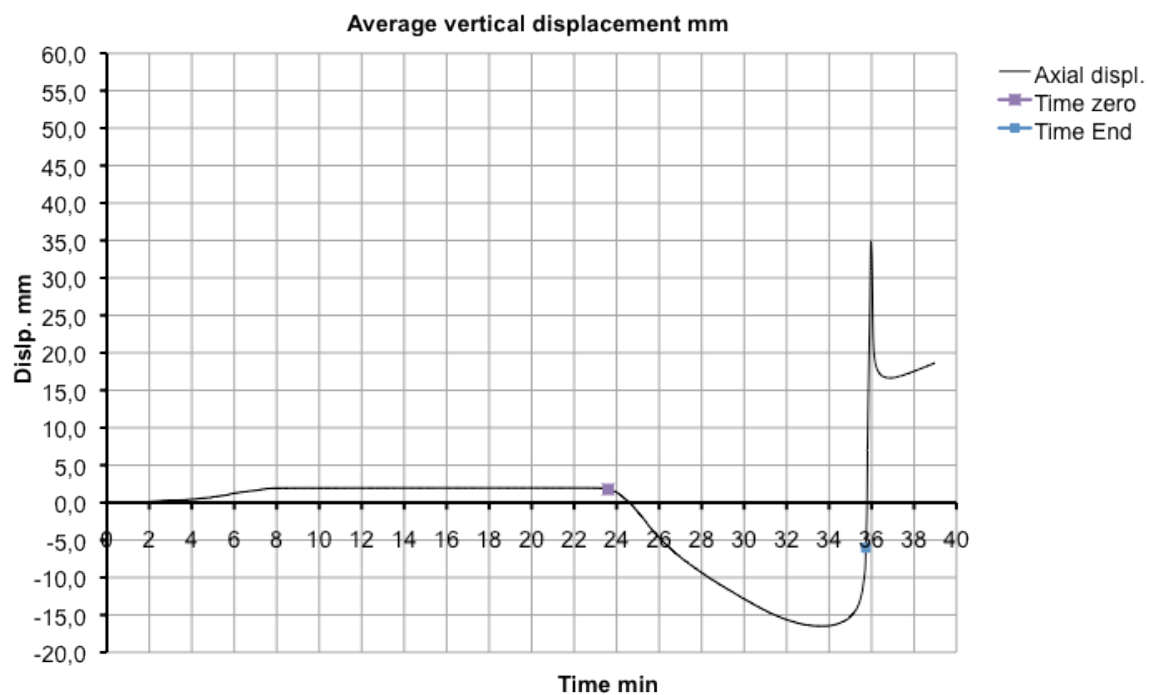


Figure 9. Average axial displacement versus time for column #1

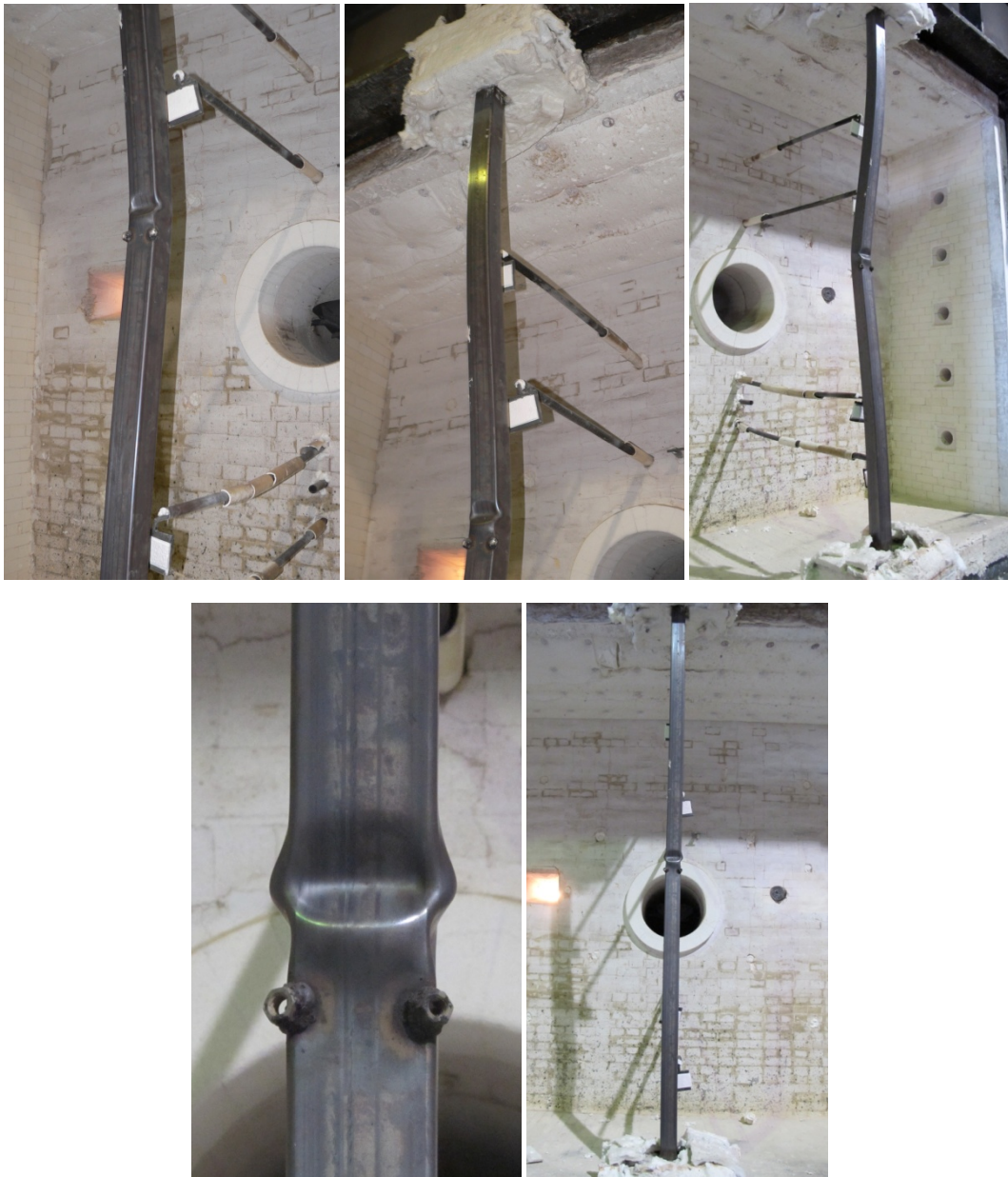


Figure 10. Failure mode for specimen #1 (3 m long)

#### 2.4.2 Column #2

Similar considerations as those made for column #1 can be drawn for column #2 too, as presented in Figure 11 to Figure 13. However, in this test the plastic hinge at the top of the column was more developed than in the previous test. The time of failure occurred at 12 min after *time zero* and at air temperature of 707.7 °C.

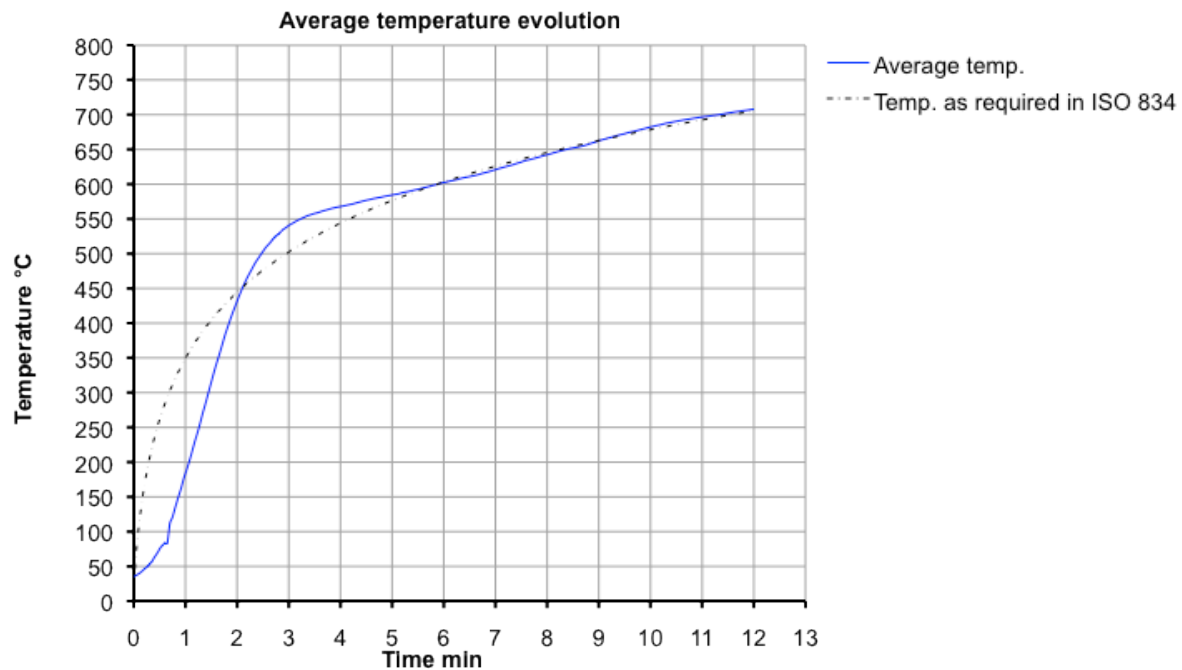


Figure 11. Average air temperature evolution for column #2

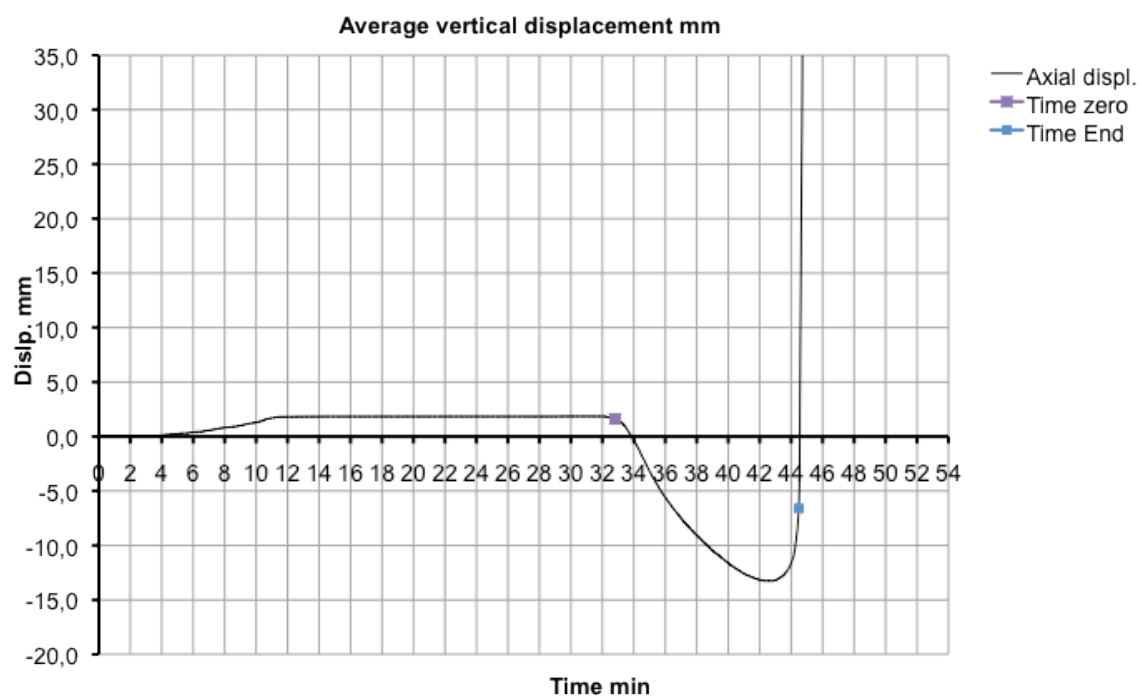


Figure 12. Average vertical displacement versus time for column #2



Figure 13. Failure mode for the column #2

#### 2.4.3 Column #3

For column #3 the time of failure occurred at 11 min 51 s after *time zero* and at the air temperature of 705 °C. Thus, in terms of fire resistance it exhibited a similar behaviour as the one experienced by column #1 and #2. As expected, it failed around its weak axis. The mode of failure was characterised by the formation of two clear plastic hinges (approximately at the top and at midspan), as shown in Figure 16. The explanation of such a behaviour is described Section 2.5.

The analysis of the transverse displacements by supposing no torsion confirmed the experimental observations. For specimen #3 bending clearly occurred about the weak axis. First, the column had a slight movement involving a major axis flexural displacement, which was quickly followed by the main movement about the weak axis.

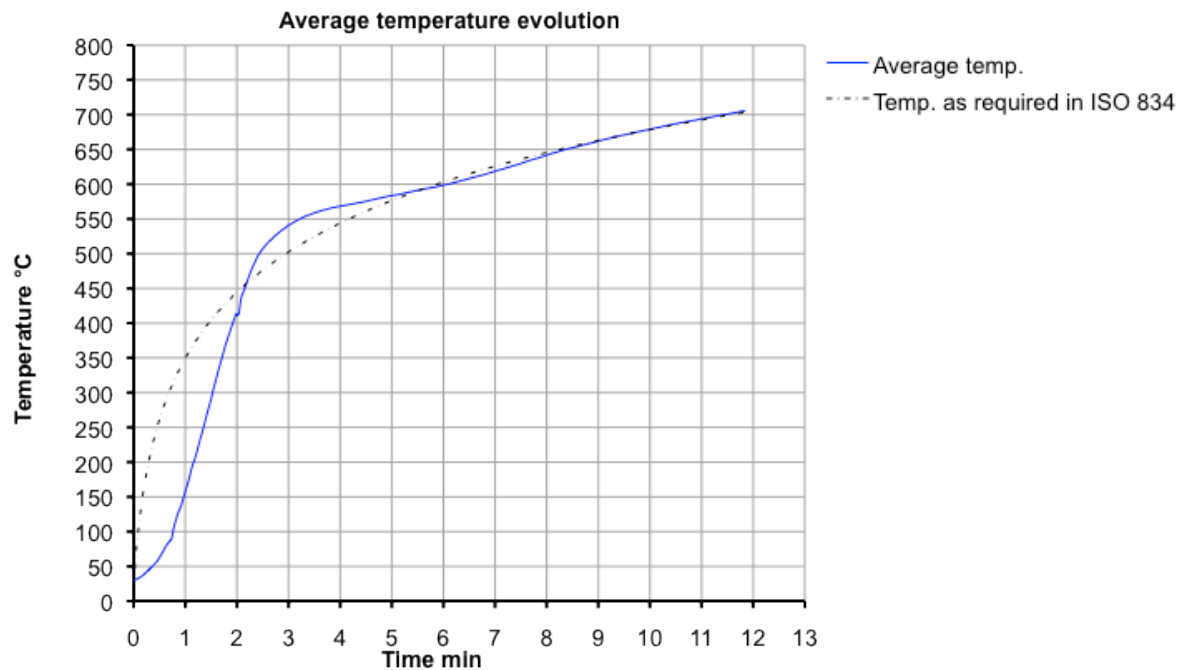


Figure 14. Average air temperature evolution for column #3

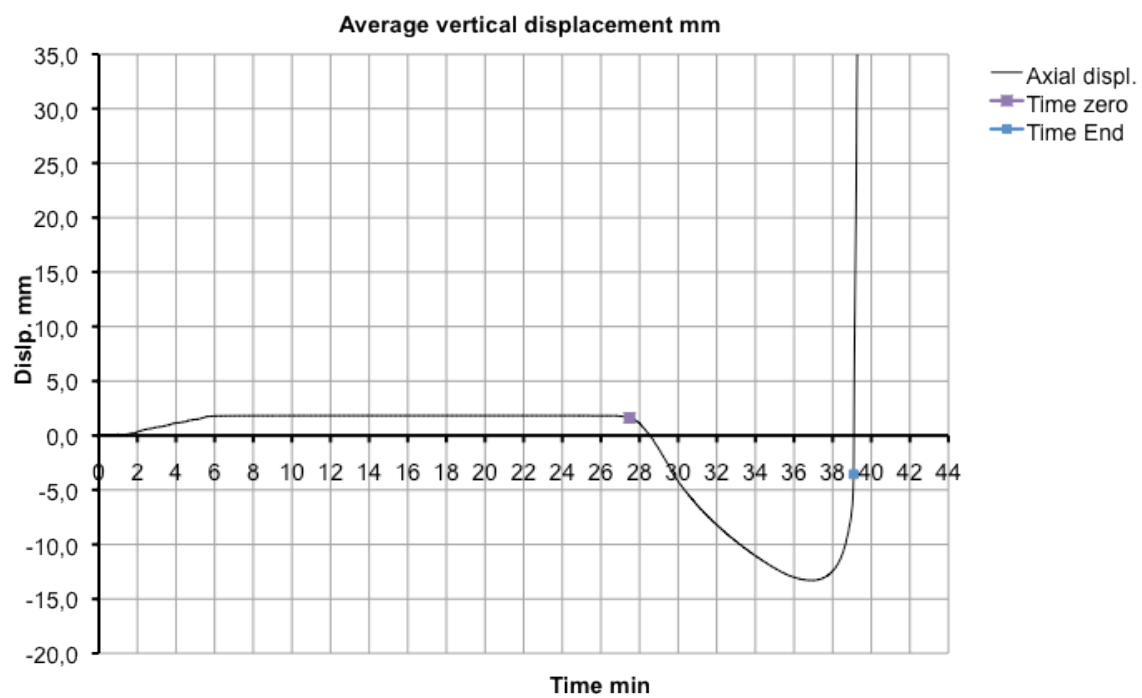


Figure 15. Average axial displacement versus time for column #3



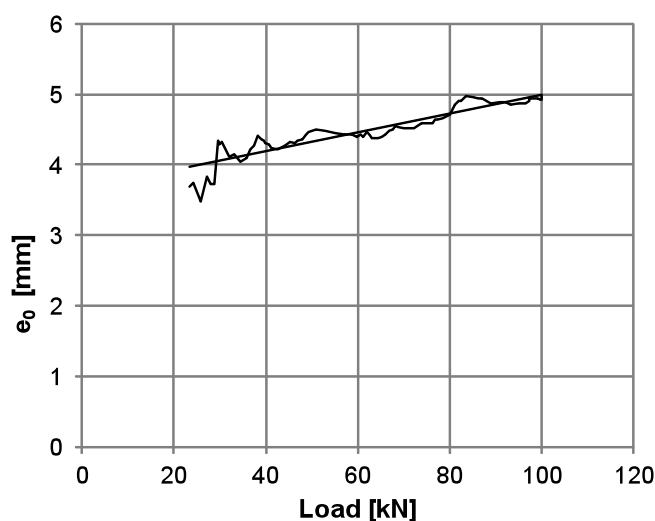


Figure 16. Failure mode for column #3

From the three tests it is possible to observe that the fire resistance was fairly the same. This was expected since the massivity factors were very similar among the specimens as well as the applied load ratio ( $0.3N_{b,Rd}$ ). Interesting to note that even though column #3 had the lowest massivity factor its fire resistance was the lowest. This is surely explicable because of a higher initial imperfection that lowered the axial capacity.

## 2.5 Analysis of the effects of temperature gradients in the member and its influence on the failure mode

From the beginning of this experimental campaign, efforts were made to achieve a *fixed-end* boundary conditions (no lateral displacements nor rotation and warping). Theoretically, in full-restrained conditions, failure would occur with an almost simultaneous formation of three plastic hinges located at the top section, at the mid-height section and at the bottom section of the column. However, in the tests it was observed the formation of two plastic hinges - at the top section and at the mid-height section - rather than three. Firstly, it was supposed that full-restrained conditions were not achieved, above all at the base section where in every tests no clear plastic hinge formed. As a partial confirmation of this hypothesis, for column #3 the initial imperfection  $e_0$  was estimated according to the Southwell diagram (Southwell, 1932) by relying on experimental data and by assuming an elastic critical load of a condition fixed-simply supported. Figure 17 shows that  $e_0$  is rather constant and comprised between 4.0 and 5.0 mm, a range of values that can be well correlated to the measured imperfection for specimen #3. However, this finding was only valid for column #3.



**Figure 17. Initial imperfection calculated using Southwell diagram for the specimen #3**

In fact, the main reason of the observed failure modes lies elsewhere. By analysing the data of the tests, it was found that the temperature in the furnace was neither uniform along the height of the columns, nor in a horizontal plane, as already observed in Tondini et al. (2013).

In particular, the top of the column was, in all tests, warmer, whereas the bottom end was always colder with a gradient along the height of about 35 °C - 40 °C in the last 30s of the test, i.e. close to failure. In the horizontal plane, at the top, the face towards the brick wall was warmer of about 22 °C - 26 °C than the face towards the closing wall; at mid-height basically no horizontal gradient appeared and; at the bottom, a gradient of about 14 °C - 24 °C between the brick wall side (hotter) and the closing wall side (colder) established. All these observations are summarised in Table 5.

On the basis of these measured temperatures, the reduction factors for yield strength of stainless steel according to EN1993-1-2 (2005) were computed: at the top, at mid-height and at the bottom sections of each column in the last 30s of each test for every faces composing the section. Each face was assumed at constant temperature based on the closest pyrometer. For the faces on the sides where no pyrometer was located, the average temperature between the furnace wall face and closing wall face was taken. By doing this it was possible to estimate the axial resistance of the column at the three sections along its height by taking into account temperature gradients. The experimental yield strength was considered (see Table 3).

From Table 5 it is possible to observe that, owing to the colder temperature at the bottom end, the estimated average axial resistance in the last 30s was significantly higher (up to 20%) than the axial resistance at mid-height and even larger with respect to that at the top section. Moreover, the estimated axial resistances at the bottom end near failure were still well higher than the applied loads (Table 4); whereas the axial resistances in the other sections were very close to them. This means that the plastic hinge at base did not form and failure occurred due to the mechanism shown in Figure 18 owing to loss of resistance caused by elevated temperatures associated with second-order effects (compare with Figure 13 and Figure 16). For column #1, the plastic hinge at the top did not clearly develop because the test was stopped soon after the first signs of instability whilst the others were pushed further.

To estimate the axial resistance the  $f_{y,t}$  according to Eq. C.1 (EN1993-1-2, 2005) was used

stainless grade		1.4003			
$f_y$ 80x80x3	458	MPa	$f_u$ 80x80x3	505	MPa
$f_y$ 120x80x3	437	MPa	$f_u$ 120x80x3	490	MPa

T [°C]	kfy	ku	k2%
600	0.45	0.42	0.45
700	0.19	0.21	0.46
800	0.13	0.12	0.47

Column #1		
B	79.6	mm
H	79.2	mm
t	2.87	mm

Column #2		
B	79.2	mm
H	79.8	mm
t	2.82	mm

Column #3		
B	119.5	mm
H	79.4	mm
t	2.97	mm

COLUMN #1						COLUMN #2						COLUMN #3					
Top section						Top section						Top section					
$T_{avg}$ last 30 s [°C]	kfy	k2%	kut	$f_{yt}$ [MPa]		$T_{avg}$ last 30 s [°C]	kfy	k2%	kut	$f_{yt}$ [MPa]		$T_{avg}$ last 30 s [°C]	kfy	k2%	kut	$f_{yt}$ [MPa]	
TC1 (Furn)	735.5	0.169	0.464	0.178	<b>83.1</b>	TC1 (Furn)	734.0	0.170	0.463	0.179	<b>83.7</b>	TC1 (Furn)	734.6	0.169	0.463	0.179	<b>80.3</b>
Tavg TC1-TC12	724.2	0.176	0.462	0.188	<b>87.2</b>	Tavg TC1-TC12	722.2	0.177	0.462	0.190	<b>87.9</b>	Tavg TC1-TC12	721.2	0.177	0.462	0.191	<b>84.9</b>
TC12 (Clos)	712.9	0.182	0.461	0.198	<b>91.2</b>	TC12 (Clos)	710.5	0.184	0.461	0.201	<b>92.0</b>	TC12 (Clos)	707.9	0.185	0.461	0.203	<b>89.5</b>
<b><math>N_{Rd}</math></b>	<b>76.6</b>	<b>kN</b>	<b>-1.31%</b>	0.99		<b><math>N_{Rd}</math></b>	<b>76.0</b>	<b>kN</b>	<b>-0.90%</b>	0.99		<b><math>N_{Rd}</math></b>	<b>97.3</b>	<b>kN</b>	<b>-1.01%</b>	0.99	
Mid section						Mid section						Mid section					
$T_{avg}$ last 30 s [°C]	kfy	k2%	kut	$f_{yt}$ [MPa]		$T_{avg}$ last 30 s [°C]	kfy	k2%	kut	$f_{yt}$ [MPa]		$T_{avg}$ last 30 s [°C]	kfy	k2%	kut	$f_{yt}$ [MPa]	
Tavg TC5-TC1 (Furn)	724.0	0.176	0.462	0.188	<b>87.2</b>	Tavg TC5-TC1 (Furn)	724.0	0.176	0.462	0.188	<b>87.2</b>	Tavg TC5-TC1 (Furn)	724.1	0.176	0.462	0.188	<b>83.9</b>
Tavg TC5-TC8	720.9	0.177	0.462	0.191	<b>88.3</b>	Tavg TC5-TC8	720.0	0.178	0.462	0.192	<b>88.7</b>	Tavg TC5-TC8	718.7	0.179	0.462	0.193	<b>85.8</b>
TC8 (Clos)	717.8	0.179	0.462	0.194	<b>89.4</b>	TC8 (Clos)	716.0	0.180	0.462	0.196	<b>90.1</b>	TC8 (Clos)	713.3	0.182	0.461	0.198	<b>87.6</b>
<b><math>N_{Rd}</math></b>	<b>77.6</b>	<b>kN</b>	-	1.00		<b><math>N_{Rd}</math></b>	<b>76.7</b>	<b>kN</b>	-	1.00		<b><math>N_{Rd}</math></b>	<b>98.3</b>	<b>kN</b>	-	1.00	
Bot section						Bot section						Bot section					
$T_{avg}$ last 30 s [°C]	kfy	k2%	kut	$f_{yt}$ [MPa]		$T_{avg}$ last 30 s [°C]	kfy	k2%	kut	$f_{yt}$ [MPa]		$T_{avg}$ last 30 s [°C]	kfy	k2%	kut	$f_{yt}$ [MPa]	
TC10 (Furn)	694.9	0.203	0.459	0.215	<b>100.1</b>	TC10 (Furn)	700.7	0.190	0.460	0.209	<b>95.5</b>	TC10 (Furn)	697.1	0.198	0.460	0.213	<b>94.5</b>
Tavg TC10-TC9	688.1	0.221	0.459	0.221	<b>105.9</b>	Tavg TC10-TC9	689.1	0.218	0.459	0.220	<b>105.0</b>	Tavg TC10-TC9	685.1	0.229	0.459	0.223	<b>104.3</b>
TC9 (Clos)	681.3	0.239	0.458	0.227	<b>111.7</b>	TC9 (Clos)	677.6	0.248	0.458	0.230	<b>114.9</b>	TC9 (Clos)	673.1	0.260	0.457	0.234	<b>114.1</b>
<b><math>N_{Rd}</math></b>	<b>93.0</b>	<b>kN</b>	<b>19.90%</b>	1.20		<b><math>N_{Rd}</math></b>	<b>90.9</b>	<b>kN</b>	<b>18.55%</b>	1.19		<b><math>N_{Rd}</math></b>	<b>119.6</b>	<b>kN</b>	<b>21.66%</b>	1.22	

Table 5. Effects of temperature gradients in the member



Figure 18. Failure mode of columns owing to a temperature gradient along the height of the column.

### 3. Preliminary comparisons with FE models

The tests were also simulated numerically by means of SAFIR: a finite element (FE) computer software developed at the University of Liège for the simulation of the behaviour of structures subjected to fire.

In this FE model, the geometry was taken as the nominal one, 80x80x3 and 120x80x3 with lengths equal to 2500 mm and 3000 mm. The corners were considered straight. SHELL elements were used to model the column. Four elements were placed within each face and a hundred along the column length implying a total number of 1600 elements (the aspect ratio ranged from 0.67 to 1.2). A global buckling imperfection of  $L/1000$  was used except for column #3 where a  $L/500$  global buckling imperfection was introduced. At this stage, no local imperfections were taken into account. The boundary conditions for all columns were supposed to be fully restrained. By doing this, the numerical simulations in terms of fire resistance were more adherent to the experimental evidences. The average tensile coupon tests results were used to model the material using the strength and deformation properties of stainless steel at elevated temperatures (Annex C EN 1993-1-2, 2005). Table C.1 of EN 1993-1-2 (2005) was used to determine the reduction factors for yield strength and elastic modulus at elevated temperature (the reference grade is 1.4003). Neither the residual stresses nor hardening due to cold forming were introduced.

These results by applying the ISO 834 curve are summarized in Table 6 and are in relatively good agreement against the test results considering that it is a preliminary study. It is worth pointing out that  $\theta_{safir}$  indicates the temperature of the furnace as in the tests where the pyrometers are located 100 mm away from the steel surface. It is advised to look at the recommendations for the boundary conditions and temperature gradients when modelling the tests using FEMs. The results of more sophisticated FE analyses will be provided in Task 4.2 under the direction of SCI.

**Table 6 Times and temperatures at failure using SAFIR**

#	1	2	3
<b>Section (mm)</b>	80 x 80 x 3	80 x 80 x 3	120 x 80 x 3
<b>Length [mm]</b>	3000.0	2500.0	2500.0
<b><math>\theta_{\text{tests}}</math> [°C]</b>	709.4	707.7	705.0
<b><math>T_{\text{tests}}</math> [min]</b>	12 min 9 s	12 min	11 min 51 s
<b><math>\theta_{\text{safir}}</math> [°C]</b>	723.8	723.8	712.1
<b><math>T_{\text{safir}}</math> [min]</b>	13 min 34 s	13 min 34 s	12 min 33 s

#### 4. Tests at room temperature

Identical columns were tested at room temperature in order to obtain the compressive axial capacities and the relative failure modes. It is worth pointing out that the three columns that were tested at ambient temperature had an initial maximum out-of-straightness less than 1 mm. In order to be fully in contact with the machine end plates, the specimen ends were cut so that the total length of each column resulted: L#1 = 2962.5 mm, L#2 = 2473.5 mm, L#3 = 2475 mm, respectively. The actual cross-section dimensions and column lengths are provided in Table 7.

The machined ends of the columns allowed for a perfect contact with the loading device. Full-restrained boundary condition was achieved during the tests (Figure 19). The column was concentrically loaded using a Schenk hydropolus whose maximum capacity is 2500 kN. The loading was displacement-controlled with speed 0.5 mm/min. Both axial and transversal displacements were measured. The global flexural transversal displacements in two perpendicular directions were measured using extensometer placed at the centre of the column (Figure 20).



**Figure 19. End plates allowing full-restrained boundary conditions**

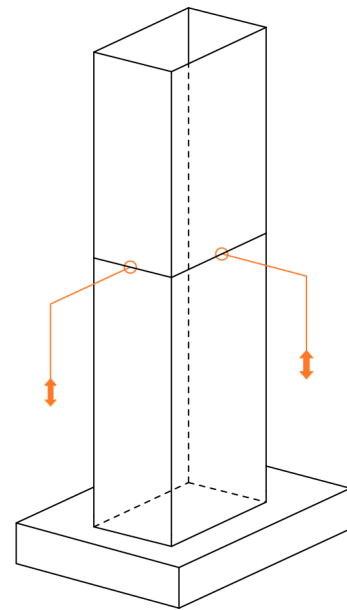




(a)



(b)



(c)

**Figure 20. Vertical system of pulleys for the measurement of the transverse displacements and corresponding transducers**

Figure 21 depicts the global behaviour of the columns in terms of axial load versus axial displacement. These tests showed that the axial capacities were higher than predicted, primarily owing to a higher average yield strength, Table 3 and Table 7).

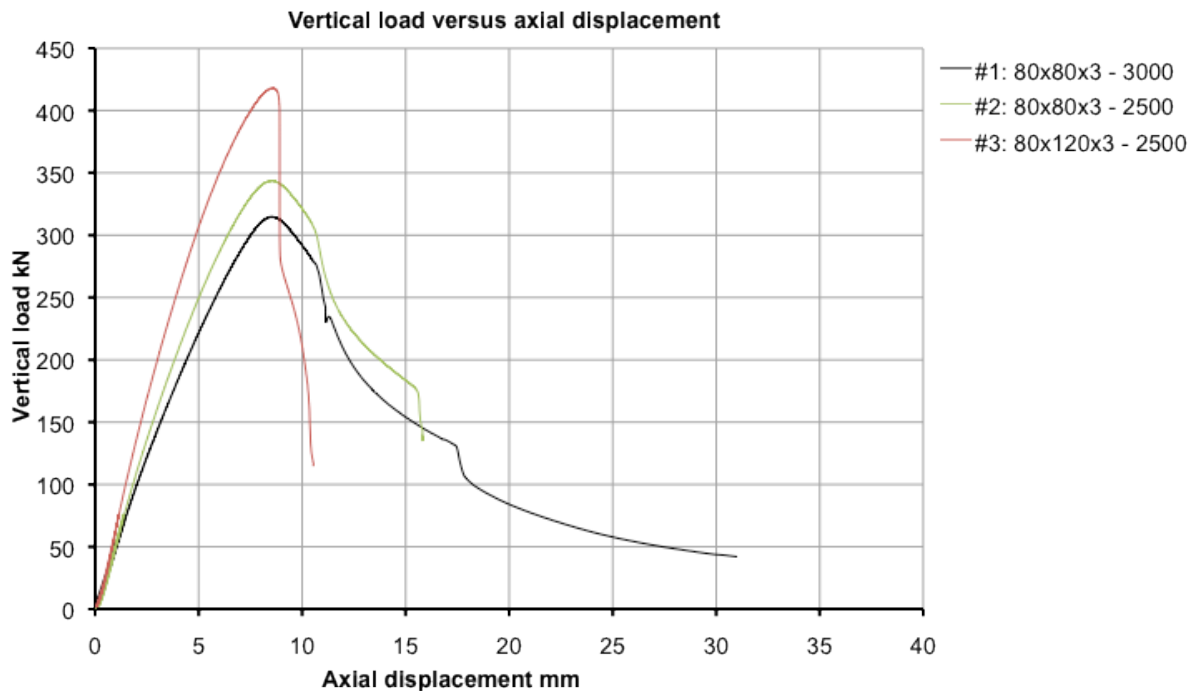


**Figure 21. Average axial displacement versus load for the specimens #1 to #3**

All the three columns failed in the same way, by combination of local buckling and global flexural buckling. During the tests it was possible to observe local buckling waves; however their amplitude was not measured. Elastic buckling firstly occurred. Then, plastic hinging appeared at midspan and at both column ends associated with increasing transverse

displacement and failure eventually occurred owing to global buckling (Figure 22). Both column ends experienced a small detached zone as well (Figure 22).

For the specimen #3 (RHS), bending occurred about the weak axis, as illustrated in Figure 23a. The assumption of no torsion was taken into account in order to compute the transverse displacements, see Figure 23b. For the SHS (columns #1 and #2), a combined flexural buckling about the two axes was detected.



**Figure 22. Post-buckling behaviour Left: Plastic mechanism in the middle of the column. Right: Plastic mechanism at the bottom end.**

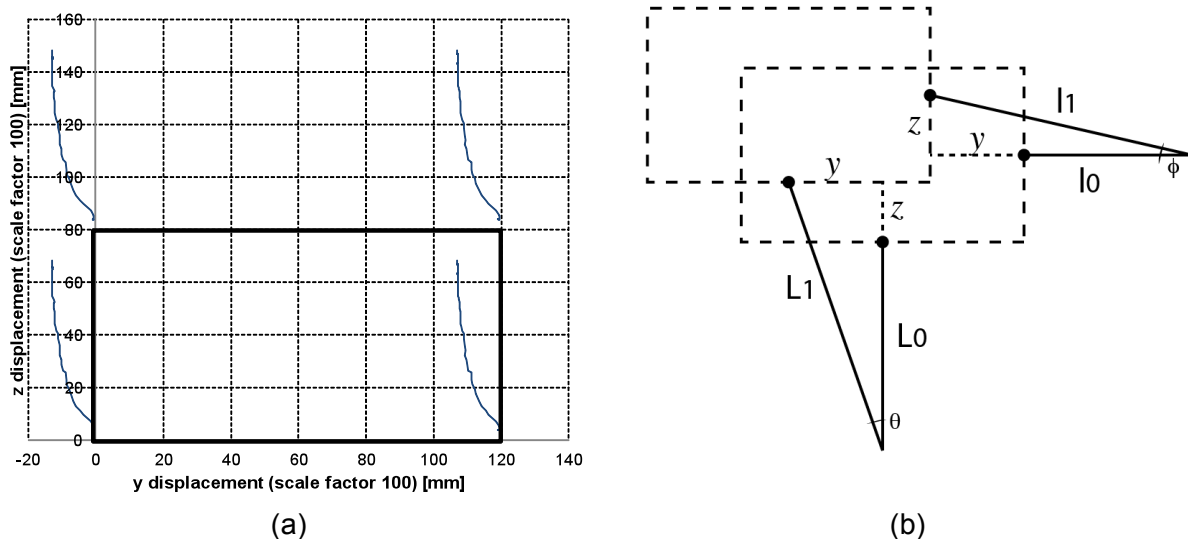


**Figure 23. a) Evolution of transverse displacements of column #3 (displacements increased by a factor of 100); b) scheme showing the assumptions to calculate transverse displacements, L1 and L0 are the measured displacements which permit the evaluation of the local coordinates**

The comparison of the force-axial displacement curves between tests at elevated temperature and tests at ambient temperature (Figure 24) clearly showed different axial stiffnesses even though their ratios should be very close to 1.0. One reason lies in the fact that the columns tested at ambient temperature were shorter, as previously described, and that the set-up at the laboratory was more flexible, owing to a much more elaborated set-up with higher deformability.

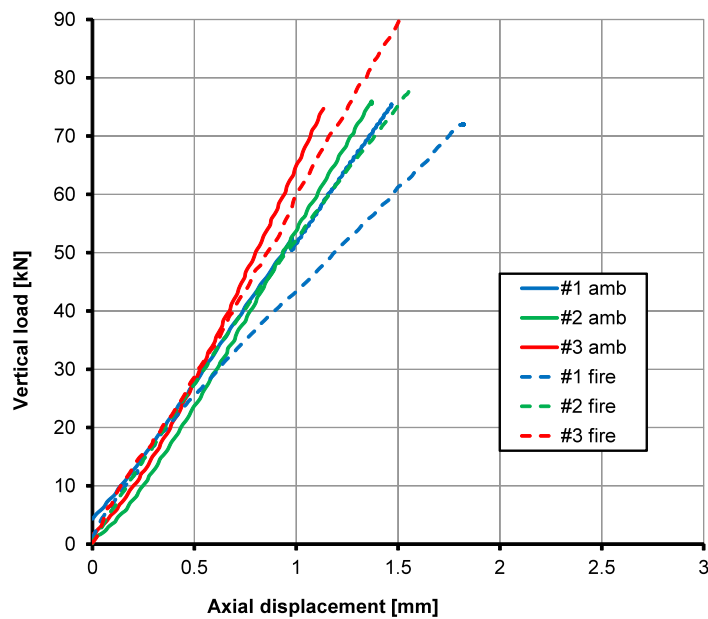


Figure 24. Comparison of vertical load-axial displacement at the beginning of loading between tests at ambient and at elevated temperature.

Table 7 Specimen dimensions (Figure 1)

#	1	2	3
Section [mm]	80 x 80 x 3	80 x 80 x 3	120 x 80 x 3
Cross-section measured dimensions [mm]	$t_{av}=2.87$ $B=79.6$ $H=79.2$	$t_{av}=2.82$ $B=79.2$ $H=79.8$	$t_{av}=2.97$ $B=79.4$ $H=119.5$
Length [mm]	2962.5	2473.5	2475.0
Maximum out-of-straightness amplitude [mm]	< L/3000	< L/2500	< L/2500
Column weight [kN]	19.5	16.3	20.7
Maximum vertical load [kN]	314.7	343.6	417.9
$N_{b,Rd}$ [kN]	239	260	336
Max. axial displ. [mm]	8.51	8.49	8.60

## 5. Global summary

Table 8 Global summary

#	1	2	3
Section [mm]	80 x 80 x 3	80 x 80 x 3	120 x 80 x 3
Cross-section measured dimensions [mm]	$t_{av} = 2.87$ $B = 79.6$ $H = 79.2$	$t_{av} = 2.82$ $B = 79.2$ $H = 79.8$	$t_{av} = 2.7$ $B = 79.4$ $H = 119.5$
<b>Material mechanical properties – 1.4003</b>			
<b>Mill certificate (Stalatube)</b>			
$\sigma_{0.2}$ [MPa]	336.0		329.0
$\sigma_{1.0}$ [MPa]	360.5		350.0
$\sigma_{ult}$ [MPa]	484.5		468.0
$\epsilon_{ult}$ [%]	42.5		37.0
<b>from Aperam, recalculated from the experimental curves</b>			
$\sigma_{0.2}$ [MPa]	458.7		437.2
$\sigma_{1.0}$ [MPa]	485.8		462.8
$\sigma_{ult}$ [MPa]	505.4		490.1
$\epsilon_{ult}$ [%]	25.6		24.2
$E_0$ [MPa]	193		194
<b>from Aperam (as provided in the technical summary)</b>			
$\sigma_{0.2}$ [MPa]	453.8		432.5
$\sigma_{1.0}$ [MPa]	485.8		462.8
$\sigma_{ult}$ [MPa]	505.2		488.1
$\epsilon_{ult}$ [%]	24.0		22.0
$E_0$ [MPa]	194.7		193.3
<b>Tests at high temperature</b>			
Maximum out-of-straightness amplitude [mm]	< L/3000	< L/2500	~L/500
Boundary conditions	Fixed	Fixed	Fixed
Length [mm]	3000.0	2499.5	2500.0
Heated length [mm]	2950.0	2449.5	2450.0
Applied load [kN]	72	78	100
Tare [kN]	9.08	10.86	10.88
$\theta_{tests}$ [°C]	709.4	707.7	705.0
$T_{tests}$ [min]	12 min 9 s	12 min	11 min 51 s
Min. axial displ. (under vert. load at ambient temp., [mm])	2.4	2.3	2.5
Max. axial displ. (dilatation, [mm])	-16.0	-12.7	-12.6

Tests at ambient temperature			
Length [mm]	2962.5	2473.5	2475.0
Maximum out-of-straightness amplitude [mm]	< L/3000	< L/2500	< L/2500
Boundary conditions	Fixed	Fixed	Fixed
Column weight [kN]	19.5	16.3	20.7
Maximum vertical load [kN]	314.7	343.6	417.9
Max. axial displ. [mm]	8.51	8.49	8.60

## 6. Conclusions

Three fire tests on thin-walled columns made of ferritic stainless steel 1.4003 were performed. Two cross sections and two lengths were taken into account. All columns were loaded with a concentric axial compression up to 30% of the design load  $N_{b,Rd}$  computed according to EN1993-1-4 (2005). Full-restrained boundary conditions were imposed. Due to similar massivity factors and applied load ratios, the fire resistance was fairly the same: about 12 minutes. The failure mode consisted of two plastic hinges and it was caused by the temperature gradient along the height developed inside the furnace.

The tests at room temperature of identical columns showed that the axial capacities were higher than predicted, primarily owing to a higher average yield strength. Moreover, they revealed discrepancies between the set-up at room temperature and that at elevated temperature by highlighting a higher deformability of the latter.


## 7. References

- EN1363-1. Fire resistance tests – Part 1: General requirement, CEN, Bruxelles; 2001.
- EN1993-1-2. Eurocode 3: Design of steel structures - Part 1-2: General rules - Structural fire design, CEN, Bruxelles; 2005.
- EN1993-1-4. Eurocode 3: Design of steel structures - Part 1-4: General rules - Supplementary rules for stainless steels, CEN, Bruxelles; 2005.
- EN 10002-1:2001. Tensile testing of metallic materials. Method of test at ambient temperature, CEN, Bruxelles; 2001.
- EN10088-2:2005. Stainless steels. Technical delivery conditions for sheet/plate and strip of corrosion resisting steels for general purposes, CEN, Bruxelles; 2005.
- ISO/IEC 17025:2005, General requirements for the competence of testing and calibration laboratories, Geneva, 2005.
- Rossi B., Afshan S., Gardner L., Strength enhancements in cold-formed structural sections – Part II: Predictive models, Journal of Constructional Steel Research, In press, 2013.
- SAFIR, A Thermal/Structural Program Modelling Structures under Fire, Franssen J.-M., Engineering Journal, A.I.S.C., Vol 42, No, 3, 143-158, 2005 <http://hdl.handle.net/2268/2928>
- Southwell R.V. On the problem of experimental observations in problems of elastic stability. Proc. R. Soc. Lond. A 135, 1932. doi: 10.1098/rspa.1932.005



Tondini N., Hoang V.L., Demonceau J.-F. and Franssen J.-M. Experimental and numerical investigation of high-strength steel circular columns subjected to fire loading. Journal of Constructional Steel Research, 80: 57-81, 2013.

## Appendix 1. Mill certificates



1/1

**INSPECTION CERTIFICATE EN 10204 3.1**

Date 03.05.2012

**Université de Liège**  
**Administration des Ressources Fin.**  
**Service Contrôle Factures**  
**Place du XX aout,7**  
**B-4000 Liege**  
**BELGIUM**

**YOUR ORDER NO.** Barbara Rossi  
**REFERENCE**  
**Laurent Faivre**

**EXTENT OF DELIVERY** **STAINLESS STEEL TUBES**

Quantity 24 m	Dimension 80x80x3,00 mm	Finish
------------------	----------------------------	--------

Heat-No. 930434	Grade of material EN 1.4003
--------------------	--------------------------------

**CHEMICAL COMPOSITION**(according to certificate of steel mill)

C %	Si %	Mn %	P %	S %	Cr %	Ni %	N %
0,012	0,260	1,430	0,032	0,002	11,300	0,400	0,010
Mo %	Ti %	Nb %	Cu %	Others %	Al %	Ca %	Mg %
-	-	-	-	-	-	-	-

**TESTING RESULTS (Coil)**

Sample-No.	YIELD STRENGTH Rp0.2 MPa	1% PROOF STRENGTH Rp1.0 MPa	TENSILE STRENGTH Rm MPa	ELONGATION A5 %	HARDNESS Hardness HB30
Test 1	339	364	488	42	173
Test 2	333	357	481	43	169

Material acc. to EN 10088-2:2005; ASTM A240-09; ASTM A554-11 (if included)


Eddycurrent test acc. to Stalatube norm. (Not applied to 'break press' tubes)

Tubes are produced according to Stalatube technical data sheet

Country of Mfg: FINLAND  
Country of Melt: FINLAND

STALATUBE OY

Lahti  
03.05.2012



Pasi Uotinen  
Quality Manager

---

**Stalatube Oy**

Ala-Okeroistentie 23, 15700 Lahti  
 FINLAND

Puh. 010 358 44 7474749  
 www.stalatube.com

Tel: +358 44 7474749  
 Fax: +358 3 882 1914

VAT FI15685444  
 Trade-Reg.No: 1568544-4



**INSPECTION CERTIFICATE EN 10204 3.1**

1/1

Date 03.05.2012

Université de Liège  
Administration des Ressources Fin.  
Service Contrôle Factures  
Place du XX aout,7  
B-4000 Liege  
BELGIUM

YOUR ORDER NO. Barbara Rossi  
REFERENCE  
Laurent Faivre

**EXTENT OF DELIVERY**

**STAINLESS STEEL TUBES**

Quantity 12 m  
Dimension 120x80x3,00 mm  
Finish

Heat-No. 904132  
Grade of material EN 1.4003

**CHEMICAL COMPOSITION**(according to certificate of steel mill)

C %	Si %	Mn %	P %	S %	Cr %	Ni %	N %
0,010	0,250	1,430	0,028	0,003	11,300	0,400	0,010
Mo %	Ti %	Nb %	Cu %	Others %	Al %	Ca %	Mg %
-	-	-	-	-	-	-	-

**TESTING RESULTS (Coil)**

Sample-No.	YIELD STRENGTH Rp0.2 N/mm2	1% PROOF STRENGTH Rp1.0 N/mm2	TENSILE STRENGTH Rm N/mm2	ELONGATION A5 %	HARDNESS HB
Test 1	329	350	468	37	27
Test 2	-	-	-	-	-

Material acc. to EN 10088-2:2005; ASTM A240-09; ASTM A554-11 (if included)

Eddycurrent test acc. to Stalatube norm. (Not applied to 'break press' tubes)

Tubes are produced according to Stalatube technical data sheet

Country of Mfg: FINLAND  
Country of Melt: FINLAND

STALATUBE OY

Lahti  
03.05.2012



Pasi Uotinen  
Quality Manager

---

Stalatube Oy

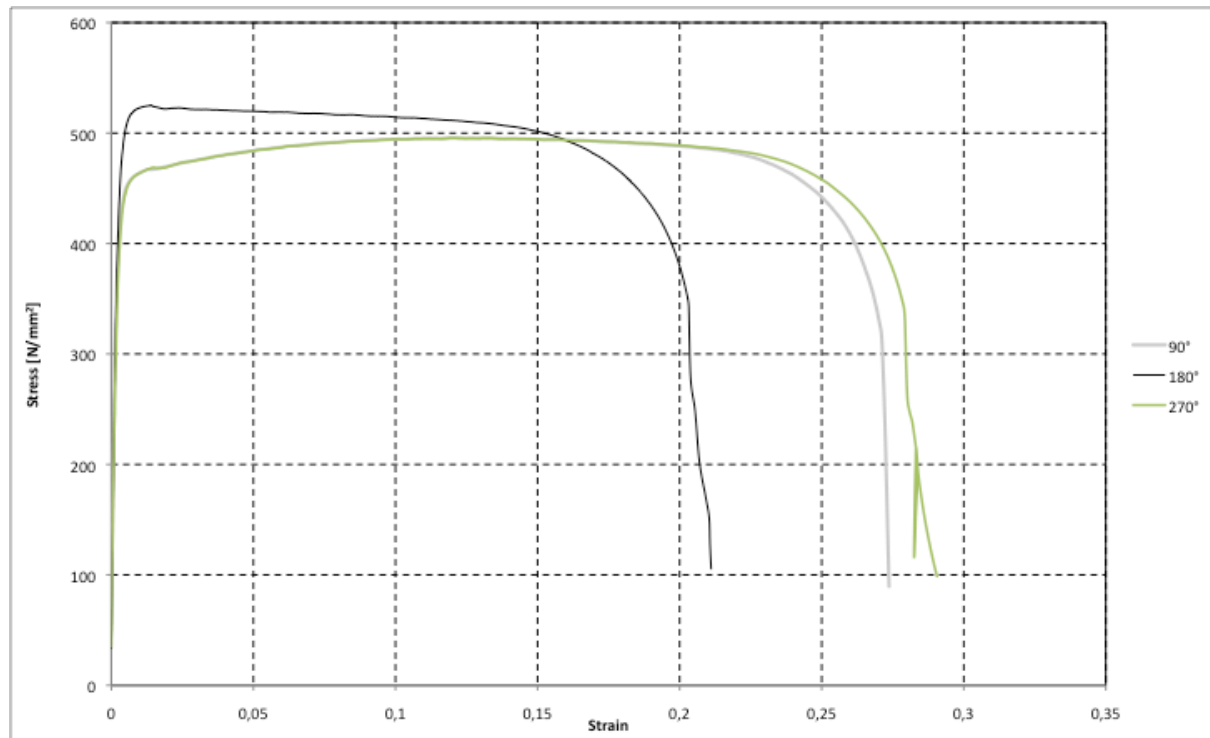
Ala-Okerointentie 23, 15700 Lahti  
FINLAND

www.stalatube.com

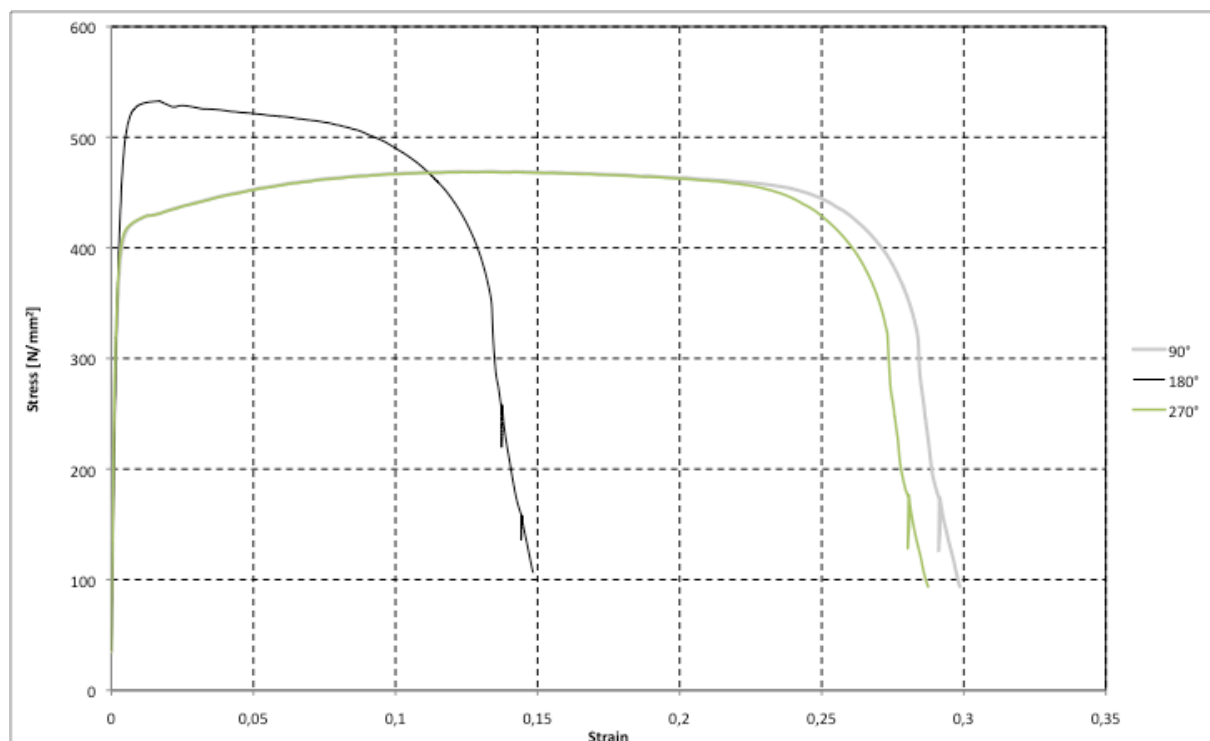
Tel: +358 44 7474749  
Fax: +358 3 882 1914

VAT FI15685444  
Trade-Reg.No: 1568544-4

## Appendix 2. Stress-strain curves

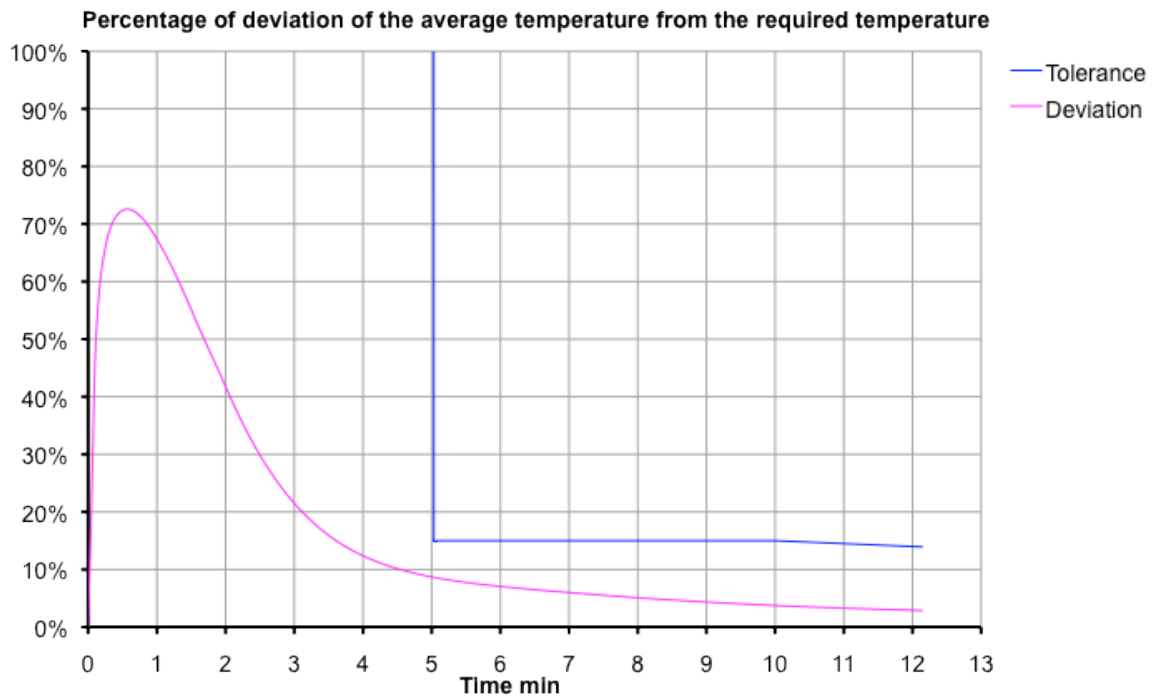


A2-1, Square Hollow section – Tensile coupon test results



A2-2, Rectangular Hollow section – Tensile coupon test results

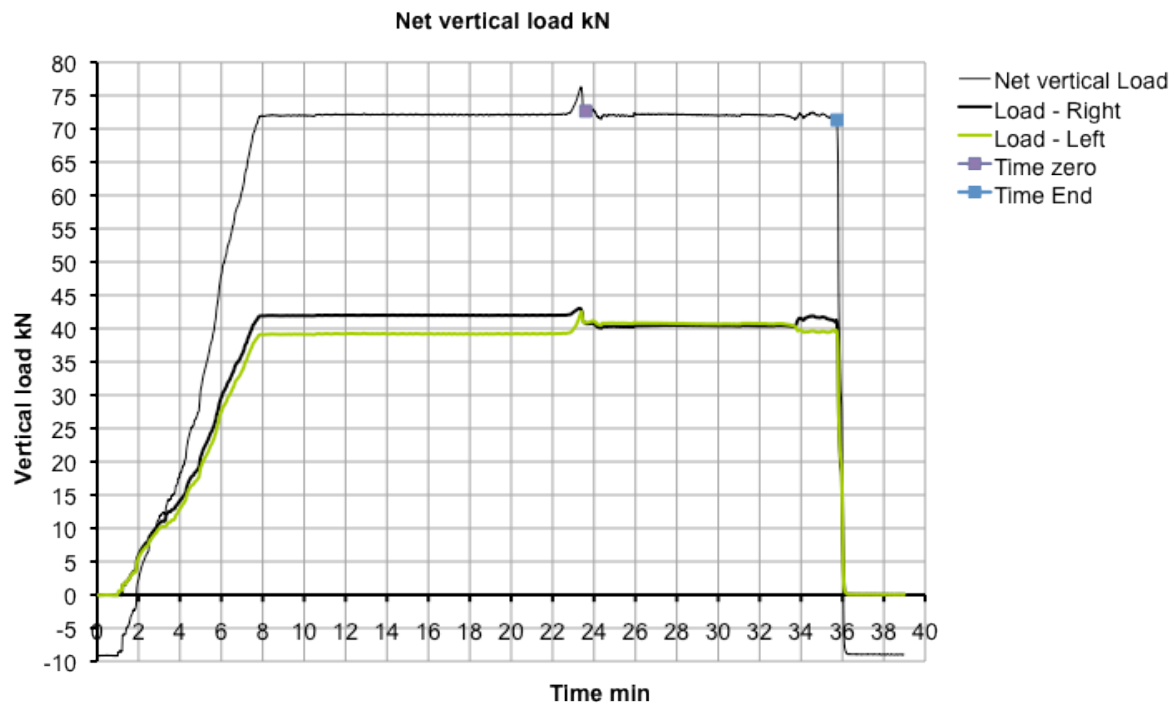
### Appendix 3. Temperature versus time curves



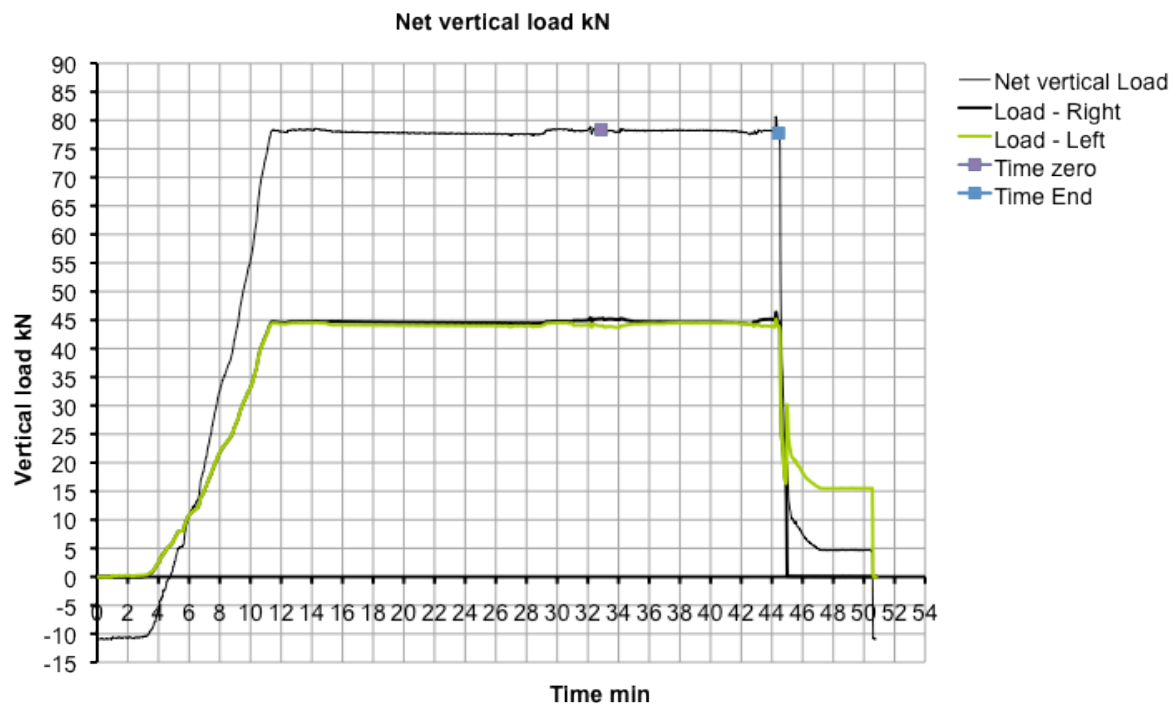
**A3-1. Average temperature deviation (from the required temperature) for specimen #1**



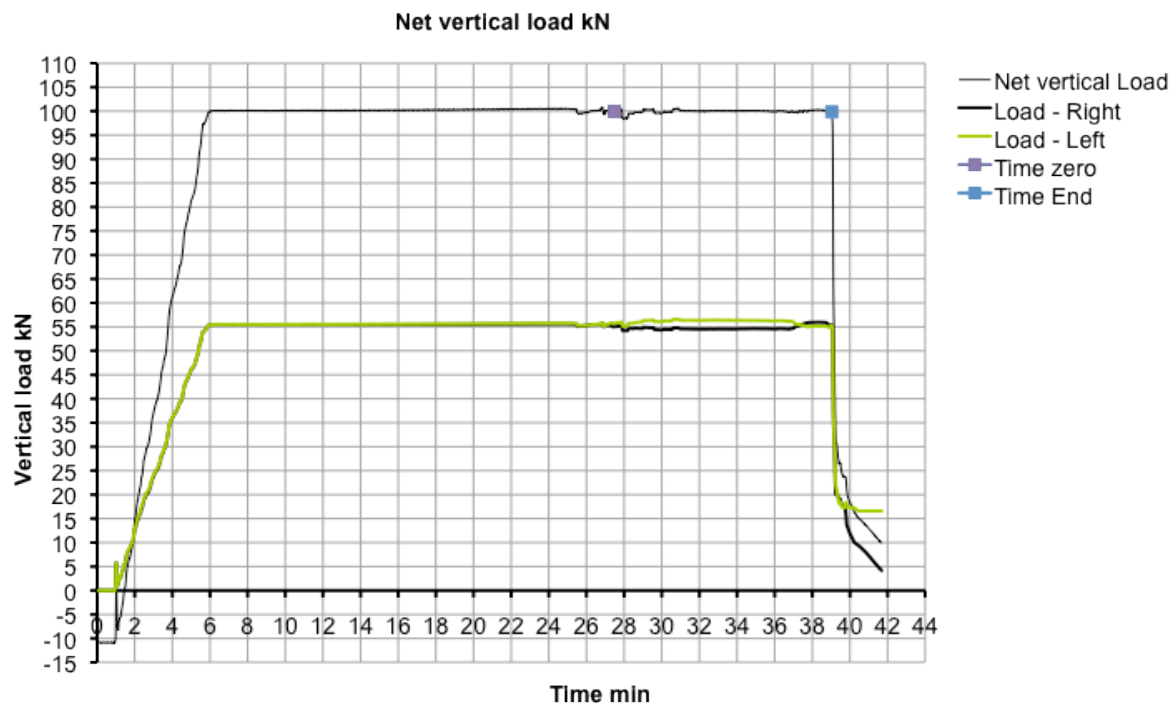
## Appendix 4. Load versus time curves



A4-1. Net vertical loads (left, right and sum minus tare) versus time for specimen #1; Time zero and Time End also indicates when the fire test occurs



A4-2. Net vertical loads (left, right and sum minus tare) versus time for the specimen #2; Time zero and Time End also indicates when the fire test occurs.



**A4-3. Net vertical loads (left, right and sum minus tare) versus time for the specimen #3; Time zero and Time End also indicates when the fire test occurs.**